Overmodulation Method With Adaptive x-y Current Limitation for Five-Phase Induction Motor Drives

Alejandro G. Yepes, *Senior Member, IEEE*, Jesús Doval-Gandoy, *Member, IEEE*

***Abstract*—Five-phase induction machines are attractive due to inherent benefits such as lower current rating than three-phase ones. On the other hand, ac motor drives often need to operate in the overmodulation (OVM) region, e.g., to increase the maximum speed or to work with reduced dc-link voltage. Most of the existing OVM strategies for five-phase drives are based on injecting low-order harmonics in the no-torque x-y plane while avoiding low-order α-β harmonics (at least up to a modulation index of 1.2311 p.u.), so as to prevent the torque ripple associated with the α-β components. However, in practice the x-y impedance is very small, and hence this approach can easily lead to overcurrent. This paper proposes an OVM method for five-phase induction motors that adaptively modifies the injected components so that at each moment the addition of low-order x-y harmonics is favored over α-β ones but without surpassing the maximum current rms of the drive. In case the total stator copper loss (SCL) tends to exceed its rating during OVM in a given scenario, the proposed scheme automatically reduces the x-y injection to keep the SCL at its rated value. Experimental results verify the theory.**

***Index Terms*—Carrier-based pulse width modulation (PWM), dc-bus utilization, multiphase ac drives, overmodulation (OVM), PWM converters, variable speed drives.**

Acronyms

OVM	Overmodulation.
PWM	Pulse width modulation.
SCL	Stator copper loss.
THD	Total harmonic distortion.
ZOH	Zero-order hold.

Variables and Symbols

∂	Partial derivative.
B_v	Bandwidth of the γ control loop when $Q=0$; $\in \mathbb{R}^+$.
B_W	Bandwidth of the γ control loop when $Q=1$; $\in \mathbb{R}^+$.
C	Matrix to obtain $\bar{v}_{xy}$ from $\bar{v}_{\alpha\beta}$ [1]; $\in \mathbb{R}^{5\text{x}5}$.
ϵ	Threshold that sets the degree of approximation for $\max\{\lvert\bar{v}_{\text{sat}}\rvert\} \approx 1$ p.u. when computing μ; $\in \mathbb{R}^+$.
$\delta_{v,\text{inst}}$	Instantaneous availability (<0) or excess (>0) of $\max\{\lvert\bar{v}_{\text{unsat}}\rvert\}$ versus 1 p.u.; when >0, it also measures the amount of necessary α-β saturation; $\in \mathbb{R}$.
δ_v	Maximum $\delta_{v,\text{inst}}$ during a fundamental period; $\in \mathbb{R}$.
$\dot{\delta}_v$	Time derivative of δ_v; $\in \mathbb{R}$.
δ_W	Adjusted measure of SCL availability (>0) or excess (<0) versus rated; $= \pm\sqrt{\lvert W^*_{xy}\rvert} - \sqrt{W_{xy}} \in \mathbb{R}$.
$\dot{\delta}_W$	Time derivative of δ_W; $\in \mathbb{R}$.
γ	Factor to adjust the x-y injection; $\in [0, \gamma_{\text{mx}}]$.
$\dot{\gamma}$	Time derivative of γ; $\in \mathbb{R}$.
γ_{mx}	Maximum allowed γ, depending on $\widehat{v}_{\alpha\beta}$; $\in [0,1]$.
i	Stator current.
$\widehat{i}_{\alpha\beta}$	Amplitude of α-β current; $= \sqrt{i_\alpha^2 + i_\beta^2} \in \mathbb{R}^+$.
$\widehat{i}_{xy}$	Amplitude of x-y current; $= \sqrt{i_x^2 + i_y^2} \in \mathbb{R}^+$.
Q	Selects between $\delta_v K_v$ (if 0) or $\delta_W K_W$ (if 1) inputs for the integrator that yields γ; $\in \{0,1\}$.
K_v	Gain for the γ control loop when $Q=0$; $\in \mathbb{R}^+$.
K_W	Gain for the γ control loop when $Q=1$; $\in \mathbb{R}^+$.
L_{ls}	Stator leakage inductance; $\in \mathbb{R}^+$.
μ	Factor to adjust (saturate) $\bar{v}_{\alpha\beta}$; $\in [0, \mu_{\text{max,o}}]$.
R_{s}	Stator resistance; $\in \mathbb{R}^+$.
s	Laplace variable; $\in \mathbb{C}$.
τ_v	Threshold for selecting Q depending on δ_v; $\in \mathbb{R}^-$.
τ_W	Threshold for selecting Q depending on δ_W; $\in \mathbb{R}^+$.
T	Transpose.
T	Vector-space-decomposition transform; $\in \mathbb{R}^{5\text{x}5}$.
T_1	Fundamental period; $= 1/f_1 \in \mathbb{R}^+$.
T_{s}	Sampling period; $\in \mathbb{R}^+$.
$\bar{v}_{\alpha\beta}$	Input vector of per-phase voltages, corresponding to only α-β fundamental voltage; $\in \mathbb{R}^5$.
$\bar{v}'_{\alpha\beta}$	Saturated $\bar{v}_{\alpha\beta}$ when $\delta_{v,\text{inst}} > 0$; $= \mu\bar{v}_{\alpha\beta} \in \mathbb{R}^5$.
$\widehat{v}_{\alpha\beta}$	Input modulation index, i.e., $\bar{v}_{\alpha\beta}$ amplitude; $\in \mathbb{R}^+$.
v_{dc}	Dc-link voltage; $\in \mathbb{R}^+$.
$\bar{v}_{\text{sat}}$	Total per-phase voltage references after α-β saturation (if any); $= \bar{v}_{\text{unsat}} \in \mathbb{R}^5$ (if $\delta_{v,\text{inst}} \le 0$); $= \bar{v}'_{\alpha\beta} + \bar{v}'_{xy} + v_{\text{zs}} \in \mathbb{R}^5$ (if $\delta_{v,\text{inst}} > 0$).
$\widehat{v}_{\text{sat},1}$	Output modulation index, i.e., amplitude of the fundamental component in $\bar{v}_{\text{sat}}$; $\in \mathbb{R}^+$.
$\bar{v}_{\text{unsat}}$	Total per-phase voltage references before α-β saturation; $= \bar{v}_{\alpha\beta} + \bar{v}'_{xy} + v_{\text{zs}} \in \mathbb{R}^5$.
$\bar{v}_{xy}$	Vector of per-phase voltages corresponding to x-y injected voltage for the method from [1]; $= C\bar{v}_{\alpha\beta} \in \mathbb{R}^5$.
$\bar{v}'_{xy}$	Adjusted $\bar{v}_{xy}$ for x-y injection; $= \gamma\bar{v}_{xy} \in \mathbb{R}^5$.
v_{zs}	Injected min-max zero-sequence voltage; $\in \mathbb{R}$.
ω_1	Fundamental frequency; $= 2\pi f_1$.
$W_{\alpha\beta}$	SCL due to α-β current, normalized by R_{s}; $\in \mathbb{R}^+$.
W_{rat}	Rated total SCL, normalized by R_{s}; $\in \mathbb{R}^+$.
W^*_{xy}	W_{xy} target to avoid SCL excess; $= W_{\text{rat}} - W_{\alpha\beta} \in \mathbb{R}$.
W_{xy}	SCL due to x-y current, normalized by R_{s}; $\in \mathbb{R}^+$.

Manuscript received December 15, 2020; revised February 22, 2021; accepted March 18, 2021. Date of publication XXXX; date of current version XXXX. This work was supported in part by the Government of Galicia under the grant ED431F 2020/07, in part by the Ministry of Science, Innovation and Universities under the Ramon y Cajal grant RYC2018-024407-I, and in part by the Spanish State Research Agency (AEI) under project PID2019-105612RB-I00/AEI/10.13039/501100011033.

A. G. Yepes and J. Doval-Gandoy are with the Applied Power Electronics Technology (APET) Research Group, Universidade de Vigo, Vigo 36310, Spain (e-mail: agyepes@uvigo.es; jdoval@uvigo.es).

Color versions of one or more of the figures in this paper are available online at http://ieeexplore.ieee.org.

Digital Object Identifier XXXX

I. Introduction

Multiphase induction motor drives offer important advantages with respect to three-phase ones, including lower phase current for given power and additional current degrees of freedom [2]–[5]. These supplementary current components can flow through extra vector-space-decomposition subspaces (x-y planes) different from the α-β plane, which, for sinusoidally distributed windings, is the only one related to electromechanical conversion [2], [3]. In particular, five-phase drives, which provide such benefits with moderate increase in phase/leg number, are especially common [1], [6]–[20].

In motor drives based on PWM, the linear modulation region of the inverter is the range of modulation-index values such that no low-order current-producing harmonics need to be injected in the α-β or x-y planes in order to synthesize a circular voltage-reference trajectory (balanced fundamental sinusoidal voltages) in the α-β plane. Zero-sequence harmonics, which do not yield current for isolated neutral points, are often injected while working in the linear modulation region to extend its range. Specifically, if the input modulation index $\widehat{v}_{\alpha\beta}$ (or simply, the modulation index) is defined as the ratio between the reference α-β voltage amplitude and $v_{\rm dc}/2$ (with $v_{\rm dc}$ being the dc-link voltage), the linear region spans from $\widehat{v}_{\alpha\beta}$ values of 0 up to $1.0515\,\mathrm{p.u.}$ for five-phase drives [12]. Operation with higher $\widehat{v}_{\alpha\beta}$ is not linear in the sense that there are low-frequency current-producing components in the output voltage that were not present in the input voltage references, and it is in general known as OVM. In ac motor drives, OVM is often crucial, e.g., so as to extend the speed operation range (e.g., for traction) [21]–[26]; if the dc-link voltage decreases (e.g., in case of faults, load increase, low capacitance, reduced power supply, etc.) [26]–[31]; for decreasing the dc-link voltage for given machine (lowering inverter loss, dead-time harmonics, electromagnetic noise, the need to use switches in series or boost dc/dc converters, etc.) [1], [32]; or for increasing the machine rated voltage for given dc-link voltage and power rating (lowering current and corresponding losses) [1], [32].

Accordingly, numerous PWM methods able to work in the OVM region have been proposed for multiphase drives. Addressing PWM while ignoring current control, as done in most of these publications, is reasonable for the sake of generality and because for induction motors open-loop V/f control is still widespread due to simplicity (e.g., speed sensors are avoided) [33]. Practically all these OVM techniques are based on injecting low-order x-y voltage harmonics while completely avoiding α-β ones, at least until the modulation index is so high that the latter is not possible (e.g., $\widehat{v}_{\alpha\beta} > 1.2311\,\mathrm{p.u.}$ for five phases). Namely, this has been done in [1], [11]–[16] for five phases, in [34]–[36] for asymmetrical six phases, in [37] for seven phases, and in [18]–[21], [32] for n-phase drives. In some of these publications special effort is devoted, e.g., to minimize current distortion [12], [13], [16], [18], to avoid common-mode voltage [13], [18], or to reduce computational burden [1], [16], [32]. Some of them rely on carrier-based PWM [1], [11], [15], [19], [20], [32], [36], some on space-vector PWM [12]–[14], [16], [18], [21], and some on either PWM type [17], [35]. In any case, all of these methods [1], [11]–[21], [32], [34]–[37] are based on adding only low-order x-y (not α-β) harmonics, as aforesaid. In general, the reasoning behind this popular strategy is that α-β harmonics produce torque ripple, whereas x-y ones only generate losses and thus are in principle highly preferable. However, in practice, since the x-y impedance (only given by the stator resistance and leakage inductance) is extremely low [1], [3], [14], [38]–[40], the added x-y harmonics can easily lead to overcurrent and damage the drive, even if the x-y voltage components are minimized for given α-β voltage reference [1], [17]. In fact, in previous papers many of these OVM methods were tested only with RL loads (with identical impedance per subspace) instead of real machines, the results were obtained with extremely low dc-link voltage, the motor parameters were not given, the motor parameters were unusually large, or the current waveforms were not shown. To ensure reasonable current magnitude during OVM, it was recently proposed to combine the x-y harmonic injection with a passive x-y filter, for five-phase [1] and n-phase drives [32]. However, the filter implies extra cost, size and weight, and it restricts the use of the extra current degrees of freedom, e.g., for fault tolerance. On the other hand, there are a few OVM approaches (e.g., for six phases [41], [42] and five-phase open-end winding drives [9]) that simultaneously inject α-β and x-y harmonics even when the former are not needed, but the proportion between them is not appropriately selected so as to achieve the best tradeoff between torque ripple and satisfaction of current limitation at each instant.

This paper presents an OVM technique for five-phase induction motor drives. The ratio between the magnitudes of the injected low-order α-β and x-y harmonics (α-β to x-y ratio) is adjusted in adaptive manner so that at each moment the value of this ratio is as low as possible without exceeding the machine rated current. Consequently, x-y voltage injection (losses) is favored over α-β injection (torque ripple), as usual, but for the first time it is done so that the current limitation is properly taken into account to avoid its violation. When the total SCL tends to surpass its rating for given conditions during OVM, the proposed strategy automatically decreases the x-y injection to preserve the drive integrity.

The rest of the paper is organized as follows. In the first place, some background fundamentals are reviewed in Section II. The proposed method is explained in Section III. Experimental results are discussed in Section IV. Finally, Section V summarizes the conclusions of the work.

II. Background

A. Vector Space Decomposition

The stator phase signals u (voltages v or currents i) can be transformed by the vector space decomposition into the α-β

plane, x-y plane and zero-sequence axis zs as [1], [3]

$$\begin{bmatrix} u_\alpha \\ u_\beta \\ u_x \\ u_y \\ u_{\rm zs} \end{bmatrix} = \overbrace{\frac{2}{5}\begin{bmatrix} 1 & \cos(\varphi) & \cos(2\varphi) & \cos(3\varphi) & \cos(4\varphi) \\ 0 & \sin(\varphi) & \sin(2\varphi) & \sin(3\varphi) & \sin(4\varphi) \\ 1 & \cos(2\varphi) & \cos(4\varphi) & \cos(6\varphi) & \cos(8\varphi) \\ 0 & \sin(2\varphi) & \sin(4\varphi) & \sin(6\varphi) & \sin(8\varphi) \\ 1/2 & 1/2 & 1/2 & 1/2 & 1/2 \end{bmatrix}}^{T} \begin{bmatrix} u_{\rm a} \\ u_{\rm b} \\ u_{\rm c} \\ u_{\rm d} \\ u_{\rm e} \end{bmatrix} \tag{1}$$

where $\varphi = 2\pi/5$.

Assuming that the stator windings are sinusoidally distributed, the x-y machine model is given by [3], [38]

$$v_x = (R_{\rm s} + sL_{\rm ls})\, i_x; \quad v_y = (R_{\rm s} + sL_{\rm ls})\, i_y \tag{2}$$

where $R_{\rm s}$ and $L_{\rm ls}$ are the stator resistance and leakage inductance, respectively. Since $R_{\rm s}$ and $L_{\rm ls}$ are typically low, even small x-y voltages can cause large x-y currents [1], [3], [14], [38]–[40]. This differs from the α-β plane, where the mutual inductance limits to a much greater extent the undesired currents [3], [38]. Moreover, the lowest harmonic order mapped into the α-β plane is the ninth one, whereas in the x-y plane it is the third one [2], [40], which also sees a smaller impedance due to the lower corresponding frequency.

B. x-y Injection for Maximum DC-Link Utilization

To maximize dc-bus exploitation in a simple manner, it has been recently proposed [1] (see Fig. 1) to sort the original per-phase modulating signals (only containing α-β components)

$$\begin{aligned} \bar{v}_{\alpha\beta} &= \begin{bmatrix} v_{\alpha\beta,{\rm a}} & v_{\alpha\beta,{\rm b}} & v_{\alpha\beta,{\rm c}} & v_{\alpha\beta,{\rm d}} & v_{\alpha\beta,{\rm e}} \end{bmatrix}^{\rm T} \\ &= T^{-1} \begin{bmatrix} v_\alpha & v_\beta & 0 & 0 & 0 \end{bmatrix}^{\rm T} \end{aligned} \tag{3}$$

from highest to lowest at each moment as $v_{\alpha\beta,1}, v_{\alpha\beta,2}, ..., v_{\alpha\beta,5}$; to obtain the respective optimum x-y terms to be injected

$$\begin{bmatrix} v_{xy,1} \\ v_{xy,2} \\ v_{xy,3} \\ v_{xy,4} \\ v_{xy,5} \end{bmatrix} = \overbrace{\begin{bmatrix} -a_1 & a_1 & 0 & a_2 & -a_2 \\ a_3 & -a_3 & 0 & a_2 & -a_2 \\ a_3 & -a_3 & 0 & -a_3 & a_3 \\ -a_2 & a_2 & 0 & -a_3 & a_3 \\ -a_2 & a_2 & 0 & a_1 & -a_1 \end{bmatrix}}^{C} \begin{bmatrix} v_{\alpha\beta,1} \\ v_{\alpha\beta,2} \\ v_{\alpha\beta,3} \\ v_{\alpha\beta,4} \\ v_{\alpha\beta,5} \end{bmatrix} \tag{4}$$

$$a_1 = 0.552786; \quad a_2 = 0.170820; \quad a_3 = 1 - a_1; \tag{5}$$

to then rearrange the resulting x-y voltages per phase as

$$\bar{v}_{xy} = \begin{bmatrix} v_{xy,{\rm a}} & v_{xy,{\rm b}} & v_{xy,{\rm c}} & v_{xy,{\rm d}} & v_{xy,{\rm e}} \end{bmatrix}^{\rm T} \tag{6}$$

by using the indices from the previous sorting; to add them to the original modulating signals $\bar{v}_{\alpha\beta}$ yielding $\bar{v}$; and to add to all phases the conventional min-max zero sequence [1], [8]

$$v_{\rm zs} = -0.5\,(\min\{\bar{v}\} + \max\{\bar{v}\}) \tag{7}$$

giving $\bar{v}'$, with which carrier-based PWM is performed. All these steps are illustrated in Fig. 1. The main harmonic in $\bar{v}_{xy}$ is of third order, with amplitude 28.95% of the $\bar{v}_{\alpha\beta}$ amplitude $\widehat{v}_{\alpha\beta}$ [1]. Compared with other five-phase OVM methods, this one is especially advantageous in terms of simplicity [1], [32].

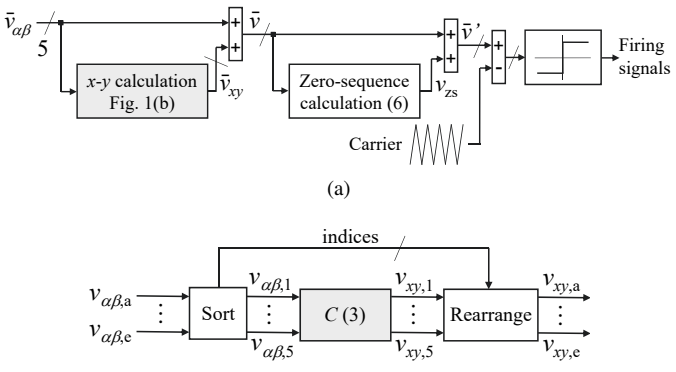

Fig. 1. Carrier-based PWM five-phase OVM method [1] with x-y and zero-sequence injection. (a) General view. (b) Calculation of $\bar{v}_{xy}$.

III. Proposed Overmodulation Method

A. General Description

The proposed five-phase OVM method is depicted in Fig. 2. The main difference with respect to previous OVM techniques for five-phase drives (e.g., that in Fig. 1), is that the novel one adaptively modifies the injected x-y components so that the machine current (or SCL) rating is not exceeded, without requiring any additional passive filters.

In Fig. 2(a), $\bar{v}_{xy}$ is computed as in Fig. 1, and the firing signals are also generated by carrier-based PWM[1]. However, unlike in Fig. 1, in Fig. 2(a) $\bar{v}_{xy}$ is multiplied (yielding $\bar{v}'_{xy}$) by a variable γ, bounded between 0 and $\gamma_{\rm mx}$, the latter of which is in turn set between 0 and 1 depending on the $\bar{v}_{\alpha\beta}$ amplitude $\widehat{v}_{\alpha\beta}$. This factor γ is generated by integration of the signals $\delta_W K_W$ or $\delta_v K_v$, depending on whether Q is 1 or 0, respectively. K_W and K_v are constants that set the integration dynamics in each case. Broadly speaking, δ_W is related to the amount by which the x-y injection can be increased without surpassing the phase-current (or SCL) rating. On the other hand, δ_v reflects the degree of voltage saturation that needs to be applied in the α-β plane after adding $\bar{v}'_{xy}$ and $v_{\rm zs}$ so that the amplitude of the final modulating signal $\bar{v}_{\rm sat}$ is not greater than that of the carrier (1 p.u.). The latter is done in the "α-β saturation" block in Fig. 2(a), which is shown in detail in Fig. 2(c). The value of Q is set according to the logic shown in Fig. 2(b). Essentially, when $\delta_W < 0$ (excessive SCL), Q becomes 1 and hence γ is reduced (or kept at 0); whereas when $\delta_W > 0$ (not excessive SCL), Q is reset to 0, increasing or decreasing γ for $\delta_v > 0$ (there is α-β saturation) or $\delta_v < 0$ (there is not), respectively. A certain hysteresis band, set by means of the thresholds τ_W and τ_v, is used in Fig. 2(c) to avoid Q chattering.

In summary, under OVM, when the SCL tends to be excessive ($\delta_W < 0$) the proposal reduces the x-y voltage injection $\bar{v}'_{xy} = \gamma \bar{v}_{xy}$ by decreasing γ through the closed-loop integration of δ_W, so that the rated SCL is not surpassed ($\delta_W \approx 0$). This is the most important novel feature. The other

[1]Without detriment to the conclusions drawn here, more advanced high-frequency switching techniques (out of scope), e.g., advanced space-vector PWM methods, could be used to produce the low-frequency voltage references $\bar{v}_{\rm sat}$ yielded by the proposal. The latter is the actual focus of this paper.

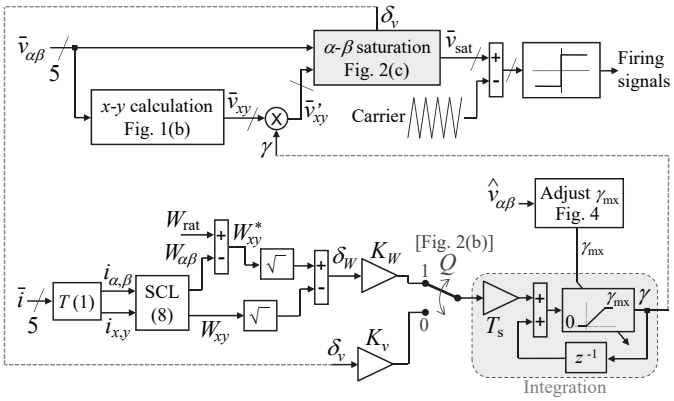

(a)

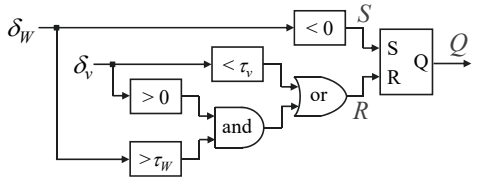

(b)

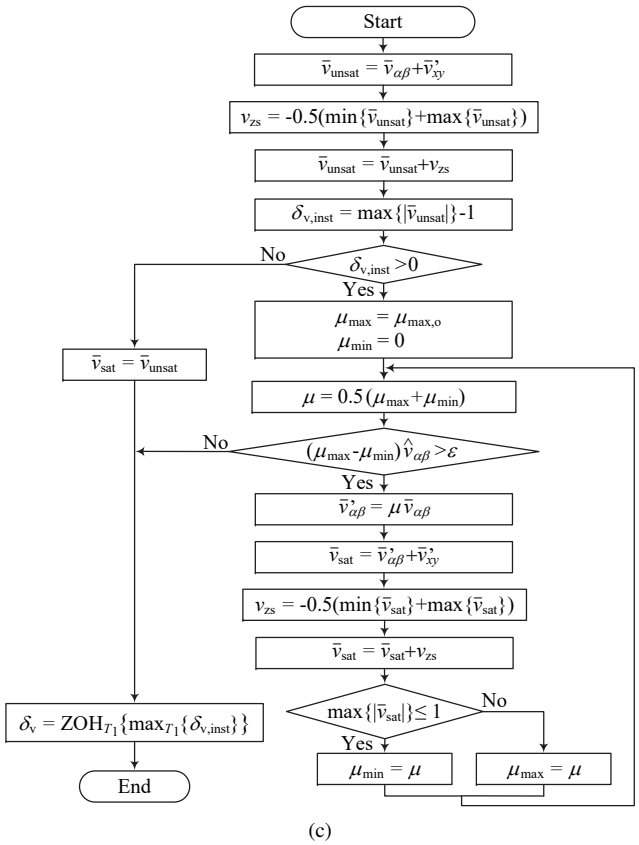

(c)

Fig. 2. Proposed five-phase OVM method. (a) General view. (b) Q logic. (c) α-β voltage saturation.

parts of Fig. 2, although necessary, are secondary with respect to this characteristic: the α-β saturation ($\delta_v > 0$) when the x-y injection is not sufficient to keep the modulating signals $\bar{v}_{\rm sat}$ within ± 1 p.u., the increase in the x-y injection (in γ) when there is α-β voltage saturation ($\delta_v > 0$) and not SCL excess ($\delta_W > 0$), the adaptation of the γ upper bound $\gamma_{\rm mx}$ to avoid other undesired effects, etc.

All these aspects are further explained next. The calculation of δ_W is addressed in Section III-B; the α-β voltage saturation and the computation of δ_v, in Section III-C; the dynamics of the γ control loop, in Section III-D; the algorithm for selecting Q using τ_v and τ_W, in Section III-E; the adjustment of the γ upper bound $\gamma_{\rm mx}$, in Section III-F; and the resulting output versus input modulation index, in Section III-G.

B. Computation of δ_W

The SCL per plane, normalized by the stator resistance, is continuously calculated [see Fig. 2(a)] using

$$W_{\alpha\beta} = (i_{\alpha,\rm rms})^2 + (i_{\beta,\rm rms})^2\,; \quad W_{xy} = (i_{x,\rm rms})^2 + (i_{y,\rm rms})^2 \tag{8}$$

where rms stands for root mean square. The squared rms values can be computed, e.g., by applying moving average filters (with window of a fundamental period $T_1 = 1/f_1 = 2\pi/\omega_1$) to the squared current signals. As illustrated in Fig. 2(a), the α-β SCL $W_{\alpha\beta}$ is subtracted from the rated total SCL $W_{\rm rat}$ to obtain the x-y SCL that can be added W^*_{xy}. Then,

$$\delta_W = \pm\sqrt{|W^*_{xy}|} - \sqrt{W_{xy}} \tag{9}$$

where the first term should be computed as a signed square root in case $W^*_{xy} < 0$, i.e., as the negative square root of $|W^*_{xy}|$. For the sake of simplicity, the $\pm$ and $||$ symbols from (9) are ignored from now on in the remaining equations. Note that, as aforementioned, $\delta_W < 0$ means excessive SCL.

It is worth remarking that δ_W in practice is here based on the total SCL rather than on the phase current because the current through each phase can be slightly different due to asymmetries. Nevertheless, the machine rated current is strongly related to the amount of losses that the machine can dissipate without damage, which is the important limitation that should be respected [6], [7]. In fact, in the ideal case of no asymmetries, SCL equal to rated ($\delta_W = 0$) implies that all the phase currents also match their rated value.

C. α-β Voltage Saturation and Computation of δ_v

As aforesaid, the magnitude of $\bar{v}'_{xy}$ is here automatically adjusted (by means of γ) during OVM so that the SCL is not excessive, in agreement with the fact that the motor impedance is much smaller in the x-y plane than in the α-β one. Thus, even if the modulation index $\widehat{v}_{\alpha\beta}$ is just slightly higher than the maximum one in the linear region ($\widehat{v}_{\alpha\beta} > 1.0515$ p.u.), certain α-β harmonics (α-β saturation) may be required to saturate the output voltage while satisfying this SCL limitation. This differs from previous OVM techniques, where α-β extra components are avoided by using relatively large x-y ones until the modulation index is so high that it is no longer possible to exclude the α-β ones ($\widehat{v}_{\alpha\beta} > 1.2311$ p.u.). In the proposed scheme, the necessary α-β harmonics are introduced (when needed) by the gray-shaded block in the upper part of Fig. 2(a), whose content is shown in detail in Fig. 2(c).

As illustrated in Fig. 2(c), the unsaturated phase-voltage references $\bar{v}_{\rm unsat}$ are first computed by adding the input α-β and x-y per-phase components $\bar{v}_{\alpha\beta}$ and $\bar{v}'_{xy}$, as well as the

zero-sequence voltage $v_{\rm zs}$, obtained by (7). The instantaneous excess of $\bar{v}_{\rm unsat}$ (denoted by $\delta_{v,\rm inst}$) is calculated as the difference of the maximum (max) of the five instantaneous $|\bar{v}_{\rm unsat}|$ values minus 1 p.u., the latter of which corresponds to the amplitude of the carrier signal. Saturation in the α-β plane is needed if and only if $\delta_{v,\rm inst} > 0$.

In case $\delta_{v,\rm inst} \leq 0$, no $\bar{v}_{\alpha\beta}$ saturation is necessary ($\bar{v}_{\rm sat} = \bar{v}_{\rm unsat}$), and the algorithm in Fig. 2(c) can be finished. Before its ending, a maximum and ZOH function is run. This function computes the maximum $\delta_{v,\rm inst}$ value (i.e., δ_v) during one fundamental cycle T_1, through multiple consecutive executions of the algorithm (one per sampling period), and the result is held during the following T_1 cycle. This is the only part of Fig. 2(c) that depends on values from previous samples.

If $\delta_{v,\rm inst} > 0$, the α-β voltage is reduced (saturated) as

$$\bar{v}'_{\alpha\beta} = \mu \bar{v}_{\alpha\beta}, \qquad \mu \in [0, \mu_{\rm max,o}]; \tag{10}$$

$$\mu_{\rm max,o} = \min\left\{1, \frac{1.2945\ \text{p.u.}}{\widehat{v}_{\alpha\beta}}\right\} \tag{11}$$

with 1.2945 p.u. being the modulus (rounded up) of the largest switching space vectors in the α-β plane [14]. The optimum μ is found in Fig. 2(c) by iteratively adjusting it until $\max\{|\bar{v}_{\rm sat|}\} \approx 1$ p.u., i.e., until the maximum absolute value of the five per-phase saturated voltages $\bar{v}_{\rm sat}$ roughly equals 1 p.u.. It can be observed that $\bar{v}_{\rm sat}$, besides $\bar{v}'_{\alpha\beta}$, also includes $\bar{v}'_{xy}$ (which does not vary with iterations) and the adapted $v_{\rm zs}$. In each iteration, μ is set as the mean between a lower and upper bound, $\mu_{\rm min}$ and $\mu_{\rm max}$, respectively. These bounds are initialized as $\mu_{\rm min} = 0$ and $\mu_{\rm max} = \mu_{\rm max,o}$ in agreement with (10), and then they are progressively made closer to each other in each iteration until the difference between them (scaled by $\widehat{v}_{\alpha\beta}$) is equal or smaller than a threshold ϵ. Said threshold establishes the degree of approximation for $\max\{|\bar{v}_{\rm sat}|\} \approx 1$ p.u.. This process of decreasing the difference between the bounds is performed by assigning μ in each iteration to either $\mu_{\rm max}$ or $\mu_{\rm min}$ depending on whether $\max\{|\bar{v}_{\rm sat}|\}$ is higher or lower than 1 p.u., respectively. The number of iterations required to converge is roughly

$$N_{\rm iter} = \text{round}\left\{0.864 - 3.3236 \log_{10}(\epsilon)\right\}. \tag{12}$$

For instance, $\epsilon = 10^{-3}$ p.u. and $\epsilon = 10^{-4}$ p.u. need only 11 and 14 iterations, respectively. Finally, once the threshold ϵ condition is met, the maximum and ZOH function related to the δ_v generation is executed before ending the algorithm, as for $\delta_{v,\rm inst} \leq 0$.

The fact that the per-phase α-β voltage is saturated according to (10) means that the space vector in the α-β plane $v_\alpha + \text{j}v_\beta$ [see (3)] is saturated by only modifying its magnitude, not its phase. This α-β saturation is analogous to the so-called minimum-phase-error approaches, which provide lowest distortion [11]. Although minimum-phase-error saturation strategies suitable for five-phase drives were used in [11], [29], they were based on reducing both α-β and x-y components by the same proportion, unlike this proposal.

D. Analysis and Design of the Dynamics of γ Control Loop

For the sake of simplicity and generality, the following analysis is carried out in the continuous domain, and it is assumed that the converter and motor are completely balanced, i.e., with no asymmetries between phases.

Two cases can be distinguished in the γ control loop, depending on whether $Q = 0$ or $Q = 1$.

1) $Q = 0$: When $Q = 0$, the integrator is driven by $\delta_v K_v$, in accordance with Fig. 2(a). Let us denote the maximum value of $\bar{v}_{\rm unsat} = \bar{v}_{\alpha\beta} + \bar{v}'_{xy} + v_{\rm zs}$ [see the top of Fig. 2(c)] per fundamental cycle by $\widehat{v}_{\rm unsat}$. Then, in steady state $\delta_v = \widehat{v}_{\rm unsat} - 1$ p.u. holds. Evaluation of these expressions in combination with the $\bar{v}_{xy}$ calculation shown in Fig. 1(b) and with $\bar{v}'_{xy} = \gamma \bar{v}_{xy}$ gives that the relation between δ_v, $\widehat{v}_{\alpha\beta}$ and the integrator output γ is given by

$$\delta_v = (0.9511 - 0.1388\gamma)\, \widehat{v}_{\alpha\beta} - 1\ \text{p.u.} \tag{13}$$

assuming steady-state, sinusoidal and balanced $\bar{v}_{\alpha\beta}$ voltages. Thus, the plant model seen by the integrator in this case is

$$\frac{\delta_v}{\gamma} = -0.1388 \widehat{v}_{\alpha\beta}. \tag{14}$$

The terms in (13) that do not depend on γ are considered as disturbances rejected in steady state and have been omitted in (14), as usually done in this type of control analysis.

The transfer function of the γ controller [see Fig. 2(a)] in continuous domain can be expressed as

$$\frac{\gamma}{\delta_v} = \frac{K_v}{s} = \overbrace{B_v \frac{\widehat{v}_{\alpha\beta}}{0.1388}}^{K_v} \frac{1}{s} \tag{15}$$

where B_v is the closed-loop bandwidth. The α-β voltage amplitude $\widehat{v}_{\alpha\beta}$, included in K_v, is straightforward to obtain from the same controller (e.g., V/f) that generates $\bar{v}_{\alpha\beta}$.

Finally, from Fig. 2, (14) and (15), the closed-loop transfer function is

$$\frac{\delta_v}{\delta_v^*} = \frac{B_v}{s + B_v} \tag{16}$$

which corresponds to a first-order low-pass filter with bandwidth B_v. The δ_v reference δ_v^* is implicitly set to $\delta_v^* = 0$ p.u. in Fig. 2. Achieving $\delta_v = \delta_v^* = 0$ means that α-β saturation is avoided during the entire fundamental period. In this manner, when $\delta_v > 0$, the proposed method attempts to bring δ_v to zero by increasing the integrator output γ, as long as $Q = 0$ holds (not excessive SCL) and $\gamma < \gamma_{\rm mx}$. In case $\delta_v < 0$, γ decreases and δ_v rises, unless γ reaches its lower bound, i.e., zero (no x-y injection).

The main constraint that should be taken into account for the B_v tuning is that δ_v is the output of a ZOH with frequency $\omega_1 = 2\pi f_1$. A common rule of thumb for control systems is that in general the bandwidth should be equal or smaller than one decade below the sampling frequency [43], [44]; thus,

$$B_v \leq \frac{\omega_1}{10}. \tag{17}$$

Setting B_v closer to this upper bound yields faster dynamics, but less robustness to uncertainties.

2) $Q = 1$: Using (2) and (8), for $Q = 1$ the plant within the γ closed loop can be modeled as

$$\frac{\sqrt{W_{xy}}}{\gamma} = \frac{\widehat{v}_{\alpha\beta}}{\sqrt{2}} \frac{0.0968}{\omega_1 L_{\mathrm{ls}}} \frac{v_{\mathrm{dc}}}{2}. \tag{18}$$

where 0.0968 is the weighted THD of the method shown in Fig. 1 [1]. For deriving (18), it is assumed that R_{s} is small compared with $\omega_1 L_{\mathrm{ls}}$. This is reasonable because OVM usually just occurs for relatively high ω_1. Moreover, the x-y disturbances that do not depend on γ (e.g., dead-time and back-electromotive-force harmonics) are rejected in steady state by the integrator and are ignored in (18).

The transfer function of the γ controller for $Q = 1$ is

$$\frac{\gamma}{\delta_W} = \frac{K_W}{s} = \overbrace{B_W \frac{\sqrt{2}}{\widehat{v}_{\alpha\beta}} \frac{\omega_1 L_{\mathrm{ls}}}{0.0968} \frac{2}{v_{\mathrm{dc}}}}^{K_W} \frac{1}{s} \tag{19}$$

where B_W is the bandwidth for the closed loop. For implementation, the $\widehat{v}_{\alpha\beta} v_{\mathrm{dc}}/2$ term in (19) can be replaced by the $\widehat{v}_{\alpha\beta}$ value without normalization, i.e., in V instead of in p.u.

Therefore, based on Fig. 2, (18) and (19), the closed-loop transfer function is

$$\frac{\sqrt{W_{xy}}}{\sqrt{W^*_{xy}}} = \frac{B_W}{s + B_W} \tag{20}$$

which is analogous to (16). Equation (20) is also equivalent to δ_W/δ^*_W, with $\delta^*_W = 0$, assuming that $\partial W_{\alpha\beta}/\partial\gamma \ll \partial W_{xy}/\partial\gamma$; the latter is reasonable, since the α-β output voltage normally does not change greatly with γ (shown in the Appendix) and, most importantly, the impedance is much smaller in the x-y plane.

In (18)-(20), the effect of the squared-rms computation for (8) by moving average filters is disregarded. Since these filters work with a window of a fundamental period T_1, to make this assumption valid

$$B_W \leq \frac{\omega_1}{10} \tag{21}$$

should be satisfied, similarly to (17). Although the dynamics imposed by (21) may seem relatively slow, in practice the maximum current (or SCL) withstood by a machine in a certain period (e.g., one second) is usually much larger than in steady state (i.e., rated) [30], [45].

E. Algorithm for Selection of $Q = 1$ or $Q = 0$

As illustrated in Fig. 2(b), Q is adjusted by means of a set-reset latch, which is driven by several logic gates and comparisons. Initially, before execution, the states of this latch and of the integrator in Fig. 2(a) (i.e., Q and γ) are zero. The thresholds τ_v and τ_W in Fig. 2(b) are constant values slightly lower and greater than zero, respectively.

Table I summarizes the main possible scenarios associated with Fig. 2(b), assuming $\tau_v \approx 0$ and $\tau_W \approx 0$. The first two columns (δ_v and δ_W signs) can be considered as the inputs based on which the other columns are derived. In particular, the δ_v and δ_W signs yield the values of S and R by using directly the circuit shown in Fig. 2(b), in turn S and R give the Q state, the δ_v and δ_W signs in combination with Q allow

TABLE I
SUMMARY OF CONDITIONS IN FIG. 2(B), ASSUMING $\tau_v \approx 0$ AND $\tau_W \approx 0$

δ_v	δ_W	S	R	Q	$\dot{\gamma}$	$\dot{\delta_v}$, $\dot{\delta_W}$
< 0	< 0	1	1	X	≤ 0	≥ 0
< 0	> 0	0	1	0	≤ 0	≥ 0
> 0	< 0	1	0	1	≤ 0	≥ 0
> 0	> 0	0	1	0	≥ 0	≤ 0

Note: overdot denotes time derivatives.

obtaining the sign of the γ time derivative $\dot{\gamma}$, and from the latter the signs of $\dot{\delta_v}$ and $\dot{\delta_W}$ follow immediately. For the last step, it is assumed that the references (e.g., W^*_{xy}) and disturbances (e.g., $\widehat{v}_{\alpha\beta}$) of the γ loop are in steady state. Note that, in accordance with (9), (13) and (18), under this assumption decreasing γ always means increasing both δ_v and δ_W, and vice versa. The signs of the time derivatives shown in Table I may not be valid at the exact instant of a transition between the conditions of two rows, but they are otherwise.

Although there are set-reset latches with set priority or with reset priority, the latch shown in Fig. 2(b) can be of either type. If the set and reset conditions are met at the same time, it means that both δ_v and δ_W are negative, and hence the integrator output decreases (or stays at zero) in any case. This is why for this situation $Q = \mathrm{X}$ is shown in Table I.

If τ_v and τ_W are set to zero in practice, undesired chattering may occur. This is especially critical regarding the last two rows of Table I, for which both Q and $\dot{\gamma}$ are modified simultaneously for a change only in the δ_W sign. For instance, if δ_W changes from positive to negative while $\delta_v > 0$, then Q switches to 1 and the time derivative of γ becomes negative; this in turn makes δ_W increase again over zero, so that then $Q = 0$, γ rises and δ_W decreases, and so on. This means that the system transitions in an oscillating manner due to the Q switching, instead of being brought smoothly to a steady state by the integrator dynamics. This behavior is prevented by means of τ_W in Fig. 2(b). Undesired continuous Q switching may also occur, despite using τ_W, if the γ values associated with $\delta_W \approx 0$ and $\delta_v \approx 0$ are similar in a certain scenario; this can be avoided by means of τ_v, as proposed in Fig. 2(b).

The flowchart of the Q selection algorithm from Fig. 2(b) without neglecting τ_v and τ_W is depicted in Fig. 3. In this diagram, reset priority is considered for the latch. A number is assigned to each of the blocks so that they can be individually referred to through the paper. The use of these thresholds τ_v and τ_W prevents the oscillation between two states with opposite values of both Q and $\dot{\gamma}$ at the same time. In fact, there are certain pairs of blocks between which transition can only occur in a single direction; namely, between blocks 1 and 4, between blocks 4 and 7, and between blocks 9 and 10.

During the initial operation of the drive (block 0, at the top of Fig. 3) usually the modulation index and the SCL are low, which implies $\delta_v < \tau_v$ and $\delta_W > \tau_W$, and thus $Q = 0$ holds. Even though the integrator input in Fig. 2(a) is negative ($\delta_v K_v < 0$), γ does not decrease, because of its lower bound (zero), and hence γ stays at zero. Consequently, the behavior of the modulating signals $\bar{v}_{\mathrm{sat}}$ is not altered by the proposed

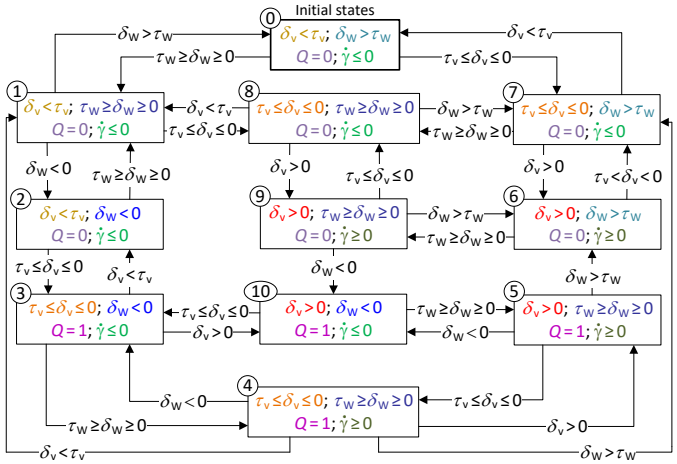

Fig. 3. Flowchart of Q selection algorithm in Fig. 2(b).

algorithm as long as $\delta_v < \tau_v$ and $\delta_W > \tau_W$.

If the peak of $\bar{v}_{\rm unsat}$ per fundamental cycle surpasses 1 p.u., then δ_v is positive [see Fig. 2(c)]. Accordingly, if in addition the SCL is lower than rated ($\delta_W > \tau_W$ and $Q = 0$), then the $\delta_v K_V > 0$ signal makes γ rise in Fig. 2(a). This corresponds with a transition between blocks $0 \rightarrow 7 \rightarrow 6$ in Fig. 3. The γ increment ($\dot{\gamma} > 0$) in turn forces δ_v and δ_W to decrease by injecting increasing x-y components [see Fig. 2]. The variable γ keeps growing until one of the following cases occur.

a) If δ_v becomes zero ($6 \rightarrow 7$ in Fig. 3), the resulting x-y injection is sufficient to avoid α-β saturation, $\bar{v}_{\rm sat}$ equals $\bar{v}_{\rm unsat}$ in Fig. 2(c), and $\dot{\gamma} = 0$ in Fig. 2(a).

b) Another possibility is that γ reaches the saturation to its upper bound $\gamma_{\rm mx}$ ($\dot{\gamma} = 0$, as well), which means that the the dc-link utilization cannot be further enhanced by injecting more x-y components, and some α-β saturation ($\delta_v > 0$) is needed in any case.

c) Alternatively, in case the SCL exceeds its rating ($W_{xy} > W^*_{xy}$), then $\delta_W < 0$ and hence $Q = 1$ is set in Fig. 2(b). This means a transition $6 \rightarrow 9 \rightarrow 10$ in Fig. 3. The input of the integrator in Fig. 2(a) changes from $\delta_v K_v$ to $\delta_W K_W < 0$, which is negative, and hence then γ tends to decrease (reducing x-y current and increasing δ_W and δ_v), unless γ is already zero (ideally null x-y current) or has settled to a steady-state value with $W_{xy} \approx W^*_{xy}$. In other words, $Q = 1$ prevents γ from growing further ($\dot{\gamma} \leq 0$), which could damage the drive.

An increase (decrease) in load torque produces an increment (decrement) in the total SCL, and hence it can also cause a transition from these conditions a) or b) to c), i.e., from $Q = 0$ to $Q = 1$ (or vice versa).

The transitions between other blocks shown in Fig. 3 could be analyzed similarly. Nonetheless, they are less relevant; e.g., it is unlikely to have $\delta_W \leq 0$ and $\delta_v \leq 0$ simultaneously, as in blocks 1, 2 and 3.

The thresholds τ_v and τ_W may be chosen for a particular application by initially setting them to very high values, and observing during operation in demanding conditions the amplitude of the oscillations in δ_v and δ_W. Then, the thresholds can be set slightly larger than such variations.

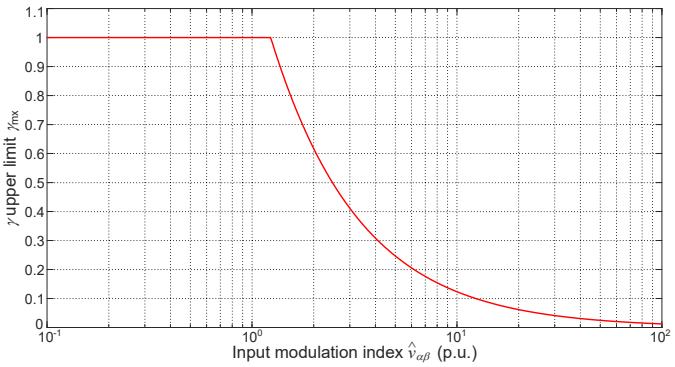

Fig. 4. Curve of the γ upper limit $\gamma_{\rm mx}$ versus the modulation index $\widehat{v}_{\alpha\beta}$, for implementing the $\gamma_{\rm mx}$ adjustment in Fig. 2(a).

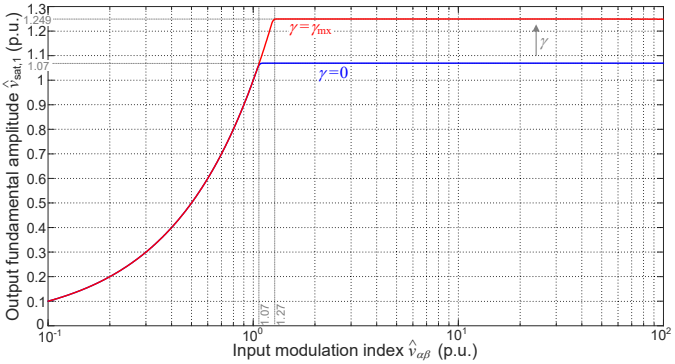

Fig. 5. Output modulation index $\widehat{v}_{\rm sat,1}$ versus input modulation index $\widehat{v}_{\alpha\beta}$, for $\gamma = \gamma_{\rm mx}$ (red) and $\gamma = 0$ (blue).

F. Adjustment of the γ Upper Limit $\gamma_{\rm mx}$

The γ factor is not allowed to exceed the upper bound $\gamma_{\rm mx}$ in the proposal [see Fig. 2(a)]. This is done because, as shown in the Appendix, for given $\widehat{v}_{\alpha\beta}$ the maximum $\widehat{v}_{\rm sat,1}$ occurs at $\gamma = \gamma_{\rm mx}$, with $\widehat{v}_{\rm sat,1}$ being the amplitude of the fundamental component of the output voltage reference $\bar{v}_{\rm sat}$, i.e., the output modulation index. In other words, $\widehat{v}_{\rm sat,1}$ rises with increasing γ when $\gamma < \gamma_{\rm mx}$, whereas the opposite occurs when $\gamma > \gamma_{\rm mx}$, the latter of which is undesired and hence avoided.

Fig. 4 shows $\gamma_{\rm mx}$ as a function of $\widehat{v}_{\alpha\beta}$. This curve is derived in the Appendix. The information represented in Fig. 4 is included as a Matlab data file in the supplementary media of the paper, and it can be implemented, e.g., as a look-up table in order to adjust $\gamma_{\rm mx}$ during operation as proposed in Fig. 2(a). From Fig. 4, $\gamma_{\rm mx}$ equals unity until $\widehat{v}_{\alpha\beta} = 1.2311$ p.u., from where it decreases progressively toward zero.

G. Output Versus Input Modulation Index

Although the complete surface of the output modulation index $\widehat{v}_{\rm sat,1}$ depending on γ and the input modulation index $\widehat{v}_{\alpha\beta}$ is shown and discussed in the Appendix, Fig. 5 shows in a compact manner $\widehat{v}_{\rm sat,1}$ versus $\widehat{v}_{\alpha\beta}$. The blue and red curves are for $\gamma = 0$ and $\gamma = \gamma_{\rm mx}$, respectively. The plots for other γ values would be in between, increasing with γ.

In the linear PWM range ($\widehat{v}_{\alpha\beta} \leq 1.0515$ p.u.), $\widehat{v}_{\rm sat,1} = \widehat{v}_{\alpha\beta}$. For $\gamma = 0$ and $\gamma = \gamma_{\rm mx}$, the highest $\widehat{v}_{\rm sat,1}$ is 1.0696 p.u. and

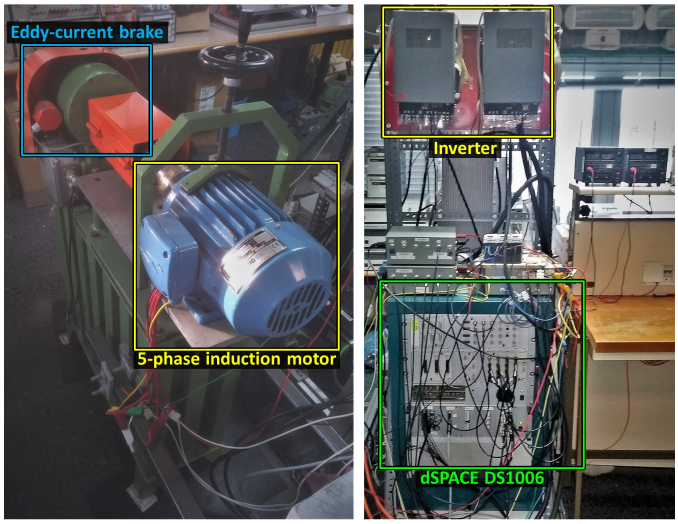

Fig. 6. Photograph of experimental setup.

1.2494 p.u., which occur roughly when $\widehat{v}_{\alpha\beta} > 1.07$ p.u. and $\widehat{v}_{\alpha\beta} > 1.27$ p.u., respectively.

IV. Experimental Results

The experimental tests are performed with a five-phase induction motor, coupled to an eddy-current brake that works as a load, as shown in Fig. 6. The machine has two pole pairs, magnetizing inductance of 530 mH, stator and rotor leakage inductance of $L_{\rm ls} = 25$ mH and $L_{\rm lr} = 50$ mH, respectively, and stator and rotor resistance of $R_{\rm s} = 9.5\,\Omega$ and $R_{\rm r} = 7\,\Omega$, respectively. The stator windings are connected in star, with isolated neutral point. Rated current of 1.273 A, rated voltage of 110 V, rated speed of 1380 r/min and rated frequency of 50 Hz are considered. Accordingly, the SCL in rated conditions is $W_{\rm rat}R_{\rm s} = 77$ W. The motor is supplied by a five-leg inverter based on insulated-gate bipolar transistors, with switching frequency of 10 kHz and dead time of 3 μs. The digital control and processing is run at 10 kHz in a dSPACE-DS1006 platform, including the DS5202 AC Motor Control Solution. Oversampling and averaging is adopted to filter the noise from the currents. Open-loop V/f control is implemented in order to generate the $\bar{v}_{\alpha\beta}$ input signals. All the results are obtained at rated frequency. The parameters of the method as selected as $\epsilon = 10^{-4}$ p.u., $K_v = K_W = 0.05\omega_1$, $\tau_v = -0.05$ p.u. and $\tau_W = 0.35$ A.

Fig. 7 shows the results at no-load condition when the dc-link voltage $v_{\rm dc}$ drops from 324 V to 253 V, i.e., the input modulation index $\widehat{v}_{\alpha\beta}$ changes from 0.96 p.u. to 1.23 p.u.. Decreasing $v_{\rm dc}$ is common for testing OVM experimentally [28]–[31], [34]–[36], and it may represent, e.g., the effect of a fault in the dc-link power supply [26], [28], [31]. The $v_{\rm dc}$ reduction is achieved by supplying the dc link by two parallel voltage sources with unequal settings, and suddenly turning one of them off. The active state corresponding to the blocks from Fig. 3 is indicated at the top of Fig. 7. During the $v_{\rm dc}$ transient $\widehat{v}_{\alpha\beta}$ rises in Fig. 7, and when it surpasses 1.0515 p.u., δ_v becomes positive. As a consequence, γ grows from zero to $\gamma_{\rm mx} = 1$, so that the x-y voltage components are entirely injected ($\bar{v}'_{xy} = \bar{v}_{xy}$) and δ_v is brought to zero. Thanks to the x-y injection it is not necessary to saturate the α-β voltage trajectory ($\delta_v \approx 0$), and hence the latter remains a circle of the same diameter in volts (greater in p.u.). The stator current, expressed as a percentage of its rated amplitude, is almost unaltered in the α-β plane and it is increased substantially in the x-y one. Nevertheless, the total SCL is still lower than rated ($\delta_W > 0$) and accordingly $Q = 0$ is maintained. The initial and final SCL and current-THD values are summarized in Table II. As a side note, the initial x-y currents in Fig. 7 are due to non-ideal effects such as back-electromotive-force and dead-time harmonics [38]–[40], the latter would be reduced if dead time were shorter [38], [40], and they are much smaller than the x-y currents due to OVM after the transient.

TABLE II
Other Measurements From the Experimental Results

Case	Initial i THD	Final i THD	Initial SCL	Final SCL
Fig. 7	9.4%	170.1%	17.2 W	64.3 W $< W_{\rm rat}R_{\rm s}$
Fig. 8	9.3%	29.8%	69.0 W	77.0 W $= W_{\rm rat}R_{\rm s}$
Fig. 9	171.4%	43.7%	65.7 W	77.0 W $= W_{\rm rat}R_{\rm s}$
Fig. 10	140.4%	87.2%	51.0 W	96.6 W $> W_{\rm rat}R_{\rm s}$

In Fig. 8 the same test is carried out, but with a certain load. Namely, in accordance with the fact that δ_W is close to zero before the $v_{\rm dc}$ transient, it can be stated that the applied load is near rated. Initally there is no OVM, i.e., no α-β or x-y harmonics are injected. Later, as $v_{\rm dc}$ drops and $\delta_v > 0$, the injected x-y components (γ) rise, but in this case Q changes to 1 as soon as the rated SCL is exceeded ($\delta_W < 0$) and then γ settles to 0.4. That is, to prevent overcurrent the proposal effectively limits the extra x-y voltage to 40%, just at the expense of some voltage distortion in the α-β plane ($\delta_v > 0$). In this manner, the SCL is kept at its rated value ($\delta_W = 0$), avoiding overheating as intended. It can also be noted that the final current THD is much lower in this case than in Fig. 7, as shown in Table II, due to the fact that the impedance is much greater in the α-β plane than in the x-y one, as expected.

The results obtained for a load step from no load to (nearly) rated torque, with $v_{\rm dc} = 253$ V ($\widehat{v}_{\alpha\beta} \approx 1.23$ p.u.), are shown in Fig. 9. This test could also be understood, roughly, as a transition from the final state of Fig. 7 to the final state of Fig. 8. The speed (not shown) drops from 1493 r/min to 1407 r/min. As the α-β current increases due to the load torque, δ_W tends to decrease in Fig. 9; nevertheless, the proposed technique adaptively reduces γ (x-y injection) down to about 0.49 so as to ensure $\delta_W = 0$, only at the cost of some α-β voltage saturation ($\delta_v > 0$). The fact that the proposal works as expected also in the case of a load increase is also in agreement with the fact that the plants of the γ control loop (14) and (18) do not depend on the load torque.

Fig. 10 shows the performance provided by the PWM OVM method from [13] for the same load step as in Fig. 9. This technique is chosen because it is claimed to provide especially low x-y current [13]. However, unlike the proposed strategy, the previous one [13] does not include adaptive x-y current limitation, and as a consequence after the torque increase the SCL exceeds the machine rated SCL by as much as 19 W (see

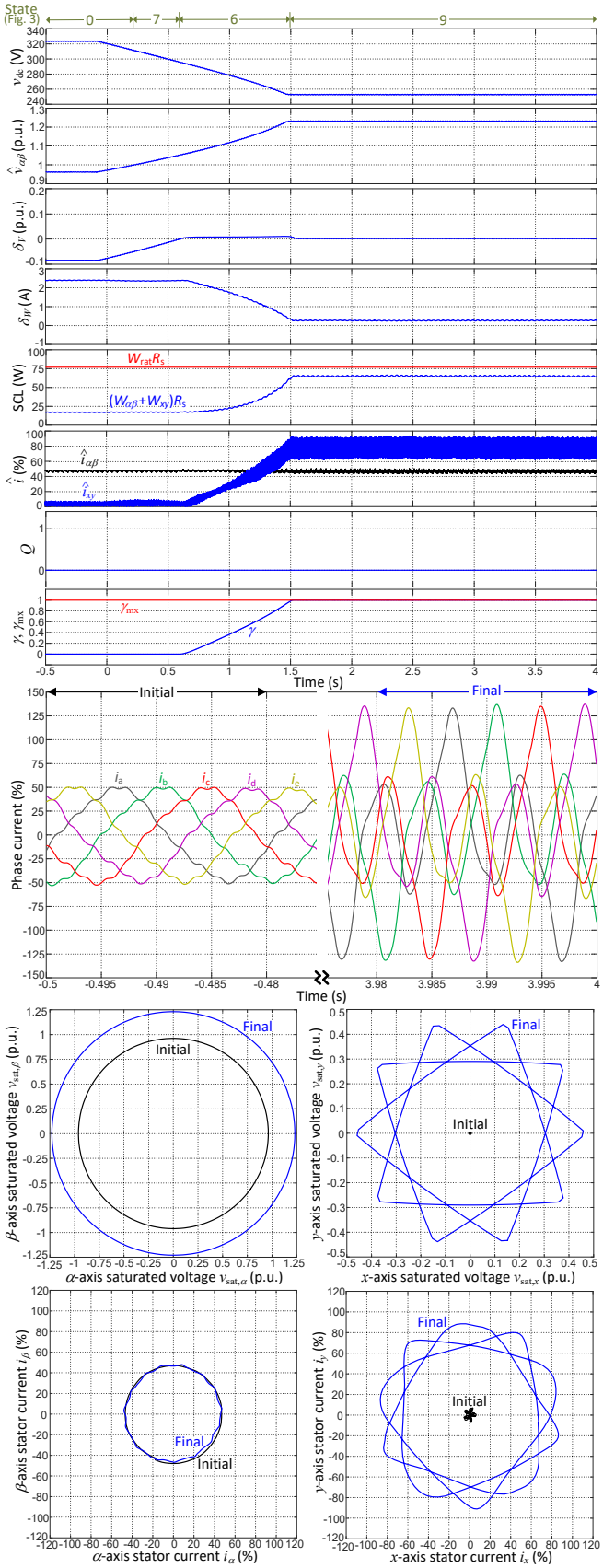

Fig. 7. Experimental behavior of the proposed method during dc-link voltage drop, for no-load condition.

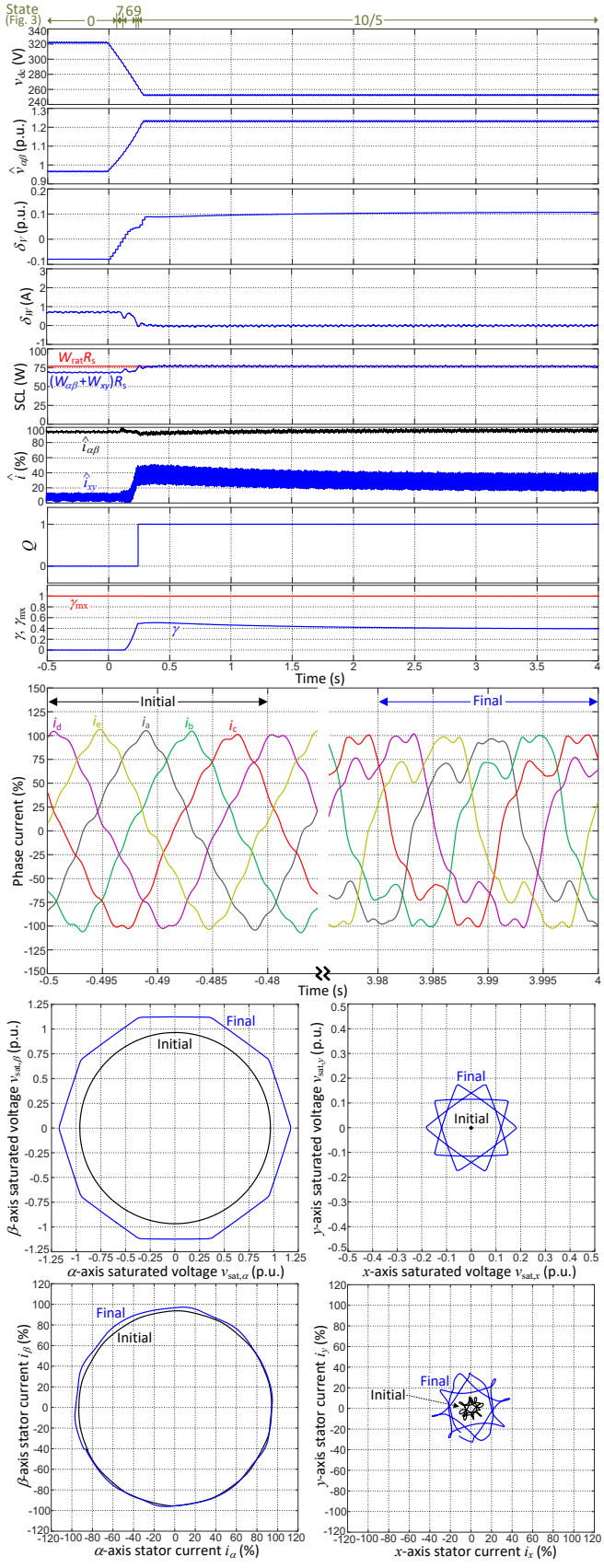

Fig. 8. Experimental behavior of the proposed method during dc-link voltage drop, near rated load.

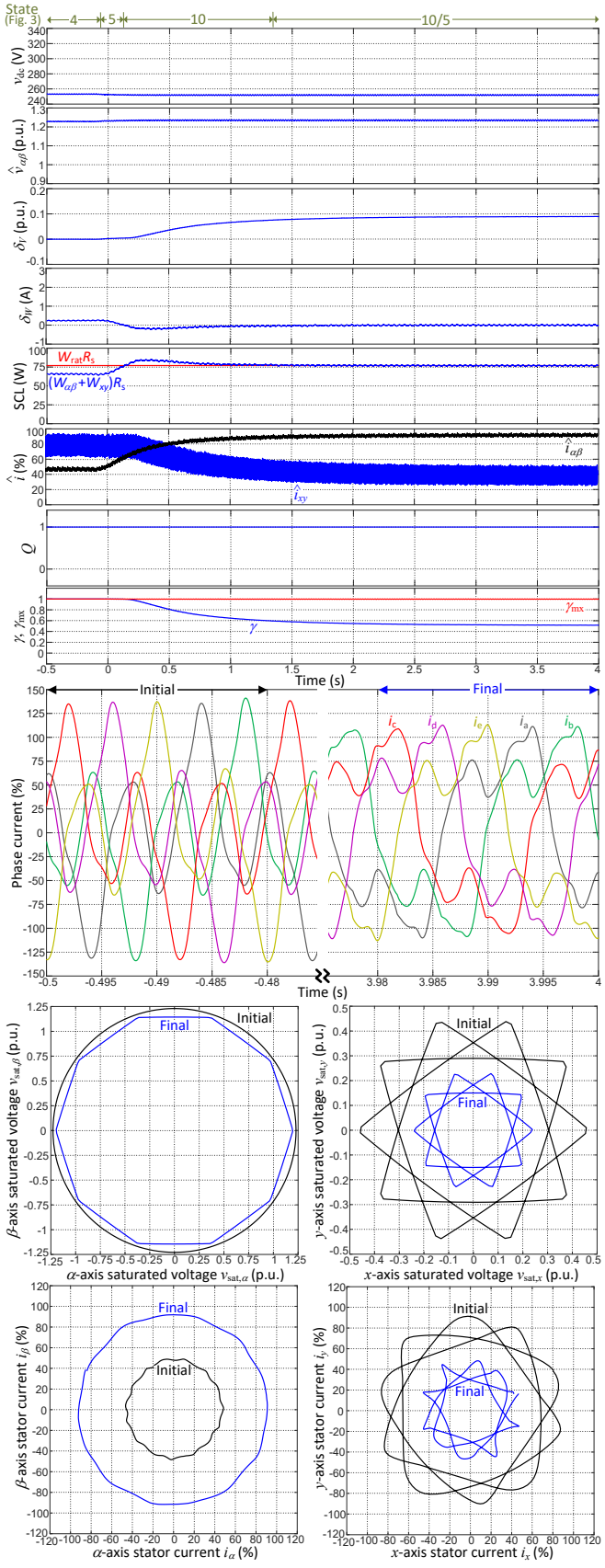

Fig. 9. Experimental behavior of the proposed method during transient from no load to rated load, for $v_{\rm dc} = 253$ V ($\widehat{v}_{\alpha\beta} \approx 1.23$ p.u.).

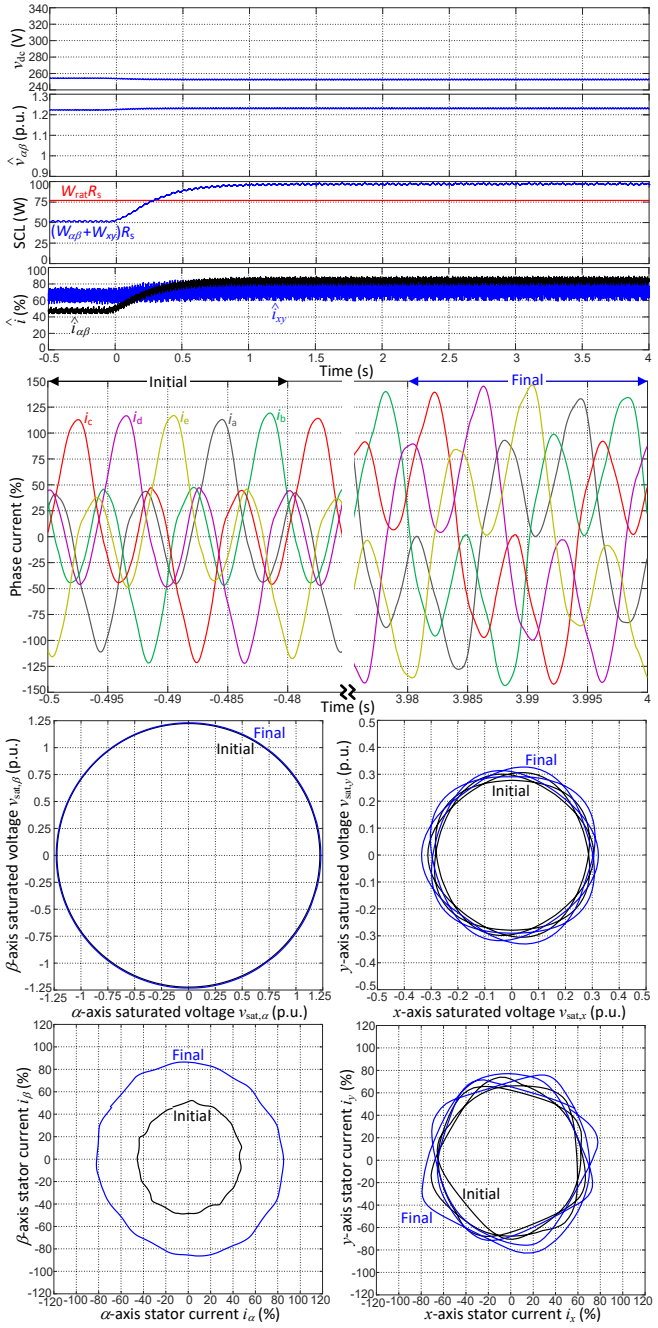

Fig. 10. Experimental behavior of the method from [13] during transient from no load to rated load, for $v_{\rm dc} = 253$ V ($\widehat{v}_{\alpha\beta} \approx 1.23$ p.u.).

Fig. 10 and Table II), compromising the drive integrity.

V. Conclusions

This paper proposes an OVM method for five-phase induction motor drives. For input modulation index above 1.0515 p.u., this strategy adaptively modifies the amount of injected low-order x-y harmonics, which typically see very small impedance, so that the machine current (or SCL) rating is not surpassed. In this manner, in contrast to existing approaches, the integrity of the drive is not compromised, and no bulky passive filters are needed for this purpose.

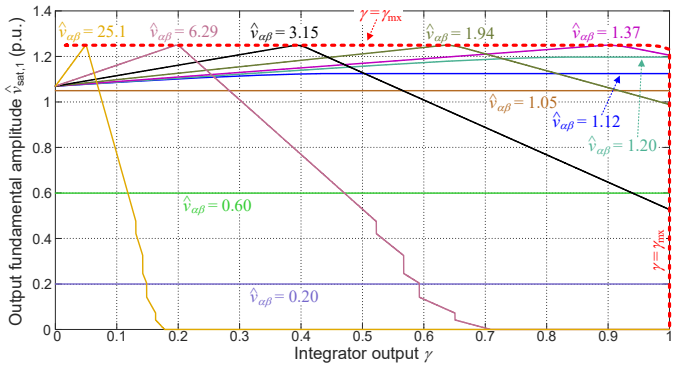

(a)

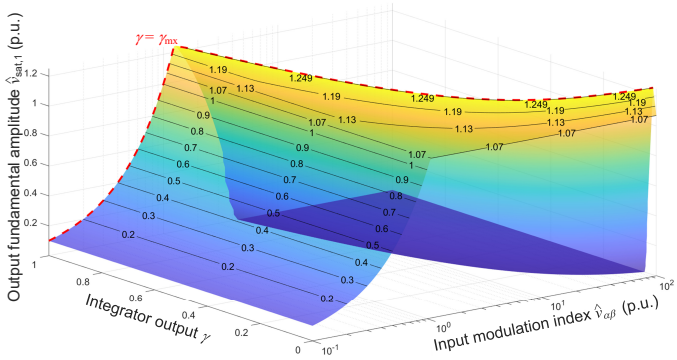

(b)

Fig. 11. Output modulation index $\widehat{v}_{\mathrm{sat},1}$ as a function of $\widehat{v}_{\alpha\beta}$ and γ. The curve of $\gamma = \gamma_{\mathrm{mx}}$ is also shown (red dashed). (a) Curves of $\widehat{v}_{\mathrm{sat},1}$ versus γ, for certain $\widehat{v}_{\alpha\beta}$ values (one per color). (b) Complete surface.

The proposal is based on an integrator whose output γ acts as a multiplying factor of the x-y components to be injected. Most importantly, the output γ of this integrator is increased by the quantity of α-β voltage saturation or decreased by the excess in measured SCL, with priority given to the latter. An algorithm is also included to saturate the α-β voltage vector with minimum phase error when the admissible x-y saturation is not sufficient. The upper limit for the integrator output γ to avoid worsening the dc-link utilization is assessed and incorporated in the scheme as a look-up table, as a function of the input modulation index.

Experimental tests, carried out with a five-phase induction machine, have verified the functionality of the proposed OVM technique in various conditions.

Subjects of potential future research include the extension/improvement of the proposal so as to work optimally for other phase numbers, during short transients, with closed-loop current/speed control, under open-circuit faults, taking into account the high-frequency switching behavior, minimizing the SCL for given modulation index, etc.

Appendix

Fig. 11 represents, as a function of γ and $\widehat{v}_{\alpha\beta}$, the output modulation index $\widehat{v}_{\mathrm{sat},1}$. Each curve in Fig. 11(a) corresponds to a value of the input $\bar{v}_{\alpha\beta}$ amplitude $\widehat{v}_{\alpha\beta}$, i.e., a section of the surface in Fig. 11(b) with a vertical plane orthogonal to the $\widehat{v}_{\alpha\beta}$ axis. As long as $\widehat{v}_{\alpha\beta} \leq 1.0515$ p.u. the PWM works in the linear region and the input and output fundamental components match in Fig. 11, i.e., $\widehat{v}_{\mathrm{sat},1} = \widehat{v}_{\alpha\beta}$. For given $\widehat{v}_{\alpha\beta}$ between 1.0515 p.u. and 1.2311 p.u. [see, e.g., the $\widehat{v}_{\alpha\beta} = 1.20$ p.u. curve in Fig. 11(a)], the output $\widehat{v}_{\mathrm{sat},1}$ increases with γ until $\widehat{v}_{\mathrm{sat},1} = \widehat{v}_{\alpha\beta}$ is reached. When $\widehat{v}_{\alpha\beta} > 1.2311$ p.u., $\widehat{v}_{\mathrm{sat},1}$ rises with γ up to $\gamma = \gamma_{\mathrm{mx}}$, and for greater γ the output $\widehat{v}_{\mathrm{sat},1}$ decreases. Since the latter is undesired, the upper limit of γ is set to γ_{mx} in the proposed method [see Fig. 2(a)]. As shown in Fig. 11, the highest output fundamental amplitude achieved in this manner is $\widehat{v}_{\mathrm{sat},1} = 1.2494$ p.u., which occurs for $\gamma = \gamma_{\mathrm{mx}}$ and roughly $\widehat{v}_{\alpha\beta} > 1.27$ p.u.. The contour lines (in black) are only shown in Fig. 11(b) for the area of the surface where the proposed method operates, i.e., for $\gamma \leq \gamma_{\mathrm{mx}}$.

Note that the curve of γ_{mx} versus $\widehat{v}_{\alpha\beta}$ shown in Fig. 4 is in agreement with the red dashed curve of Fig. 11. In addition, the plots of $\widehat{v}_{\mathrm{sat},1}$ versus $\widehat{v}_{\alpha\beta}$ in Fig. 5 are consistent with the $\gamma = \gamma_{\mathrm{mx}}$ and $\gamma = 0$ lines in Fig. 11.

References

[1] A. G. Yepes, J. Doval-Gandoy, and H. Toliyat, "Improvement in dc-link utilization with reduced current and torque deterioration for five-phase drives by combination of circulating-current filters and simple carrier-based PWM based on closed-form expressions," *IEEE Trans. Ind. Electron.*, vol. 68, no. 2, pp. 960–971, Feb. 2021.

[2] E. Levi, "Multiphase electric machines for variable-speed applications," *IEEE Trans. Ind. Electron.*, vol. 55, no. 5, pp. 1893–1909, May 2008.

[3] E. Levi, R. Bojoi, F. Profumo, H. A. Toliyat, and S. Williamson, "Multiphase induction motor drives—A technology status review," *IET Electr. Power Appl.*, vol. 1, no. 4, pp. 489–516, Jul. 2007.

[4] F. Barrero and M. J. Duran, "Recent advances in the design, modeling and control of multiphase machines—Part 1," *IEEE Trans. Ind. Electron.*, vol. 63, no. 1, pp. 449–458, Jan. 2016.

[5] M. Duran and F. Barrero, "Recent advances in the design, modeling and control of multiphase machines—Part 2," *IEEE Trans. Ind. Electron.*, vol. 63, no. 1, pp. 459–468, Jan. 2016.

[6] A. S. Abdel-Khalik, A. S. Morsy, S. Ahmed, and A. M. Massoud, "Effect of stator winding connection on performance of five-phase induction machines," *IEEE Trans. Ind. Electron.*, vol. 61, no. 1, pp. 3–19, Jan. 2014.

[7] A. S. Abdel-Khalik, M. A. Elgenedy, S. Ahmed, and A. M. Massoud, "An improved fault-tolerant five-phase induction machine using a combined star/pentagon single layer stator winding connection," *IEEE Trans. Ind. Electron.*, vol. 63, no. 1, pp. 618–628, Jan. 2016.

[8] E. Levi, D. Dujic, M. Jones, and G. Grandi, "Analytical determination of dc-bus utilization limits in multiphase VSI supplied ac drives," *IEEE Trans. Energy Convers.*, vol. 23, no. 2, pp. 433–443, Jun. 2008.

[9] M. Priestley, J. E. Fletcher, and C. Tan, "Space-vector PWM technique for five-phase open-end winding PMSM drive operating in the overmodulation region," *IEEE Trans. Ind. Electron.*, vol. 65, no. 9, pp. 6816–6827, 2018.

[10] A. Iqbal and S. Moinuddin, "Comprehensive relationship between carrier-based PWM and space vector PWM in a five-phase VSI," *IEEE Trans. Power Electron.*, vol. 24, no. 10, pp. 2379–2390, Oct. 2009.

[11] L. Vancini, M. Mengoni, G. Rizzoli, G. Sala, L. Zarri, and A. Tani, "Carrier-based PWM overmodulation strategies for five-phase inverters," *IEEE Trans. Power Electron.*, vol. 36, no. 6, pp. 6988–6999, 2021.

[12] G. Carrasco and C. Silva, "Space vector PWM method for five-phase two-level VSI with minimum harmonic injection in the overmodulation region," *IEEE Trans. Ind. Electron.*, vol. 60, no. 5, pp. 2042–2053, May 2013.

[13] M. J. Duran, J. Prieto, and F. Barrero, "Space vector PWM with reduced common-mode voltage for five-phase induction motor drives operating in overmodulation zone," *IEEE Trans. Power Electron.*, vol. 28, no. 8, pp. 4030–4040, Aug. 2013.

[14] A. Iqbal and E. Levi, "Space vector modulation schemes for a five-phase voltage source inverter," in *Proc. EPE*, Sep. 2005, pp. 1–12.

[15] T. Komrska, T. Glasberger, and Z. Peroutka, "Carrier-based PWM with minimum infinity norm for overmodulation area of five-phase converters," in *Proc. EPE ECCE*, Sep. 2016, pp. 1–8.

[16] F. Bu, T. Pu, Q. Liu, B. Ma, M. Degano, and C. Gerada, "Four-degree-of-freedom overmodulation strategy for five-phase space vector pulsewidth modulation," *IEEE J. Emerg. Sel. Topics Power Electron.*, vol. 9, no. 2, pp. 1578–1590, 2021.
[17] S. Halasz, "Overmodulation region of multi-phase inverters," in *Proc. EPE-PEMC*, Sep. 2008, pp. 682–689.
[18] J. Prieto, F. Barrero, M. J. Duran, S. Toral Marin, and M. A. Perales, "SVM procedure for n-phase VSI with low harmonic distortion in the overmodulation region," *IEEE Trans. Ind. Electron.*, vol. 61, no. 1, pp. 92–97, Jan. 2014.
[19] A. Iqbal, E. Levi, M. Jones, and S. N. Vukosavic, "Generalised sinusoidal PWM with harmonic injection for multi-phase VSIs," in *Proc. IEEE PESC*, Jun. 2006, pp. 1–7.
[20] T. Komrska, T. Glasberger, and Z. Peroutka, "Universal PWM modulator for multiphase drives with a minimum infinity-norm approach," *IEEE Trans. Ind. Electron.*, vol. 63, no. 10, pp. 5979–5987, Oct. 2016.
[21] P. Young and M. Preindl, "Optimal generalized overmodulation for multiphase PMSM drives," in *Proc. IEEE APEC*, Mar. 2017, pp. 500–505.
[22] S. K. Sahoo and T. Bhattacharya, "Rotor flux-oriented control of induction motor with synchronized sinusoidal PWM for traction application," *IEEE Trans. Power Electron.*, vol. 31, no. 6, pp. 4429–4439, 2016.
[23] A. Ghaderi, T. Umeno, and M. Sugai, "An altered PWM scheme for single-mode seamless control of ac traction motors for electric drive vehicles," *IEEE Trans. Ind. Electron.*, vol. 63, no. 3, pp. 1385–1394, Mar. 2016.
[24] K. Sun, Q. Wei, L. Huang, and K. Matsuse, "An overmodulation method for PWM-inverter-fed IPMSM drive with single current sensor," *IEEE Trans. Ind. Electron.*, vol. 57, no. 10, pp. 3395–3404, Oct. 2010.
[25] S. K. Giri, S. Mukherjee, S. Kundu, S. Banerjee, and C. Chakraborty, "An improved PWM scheme for three-level inverter extending operation into overmodulation region with neutral-point voltage balancing for full power-factor range," *IEEE J. Emerg. Sel. Topics Power Electron.*, vol. 6, no. 3, pp. 1527–1539, 2018.
[26] X. Zhang and G. H. B. Foo, "Overmodulation of constant-switching-frequency-based DTC for reluctance synchronous motors incorporating field-weakening operation," *IEEE Trans. Ind. Electron.*, vol. 66, no. 1, pp. 37–47, Jan. 2019.
[27] D. Casadei, M. Mengoni, G. Serra, A. Tani, and L. Zarri, "A control scheme with energy saving and dc-link overvoltage rejection for induction motor drives of electric vehicles," *IEEE Trans. Ind. Appl.*, vol. 46, no. 4, pp. 1436–1446, Jul. 2010.
[28] S. Kim and J. Seok, "Induction motor control with a small dc-link capacitor inverter fed by three-phase diode front-end rectifiers," *IEEE Trans. Power Electron.*, vol. 30, no. 5, pp. 2713–2720, May 2015.
[29] A. G. Yepes, J. Doval-Gandoy, and H. A. Toliyat, "Multifrequency current control for n-phase machines including antiwindup and distortion-free saturation with full dc-bus utilization," *IEEE Trans. Power Electron.*, vol. 34, no. 10, pp. 9891–9905, Oct. 2019.
[30] A. G. Yepes and J. Doval-Gandoy, "Effective current limitation for multifrequency current control with distortion-free voltage saturation and antiwindup," *IEEE Trans. Power Electron.*, vol. 35, no. 12, pp. 13 697–13 713, Dec. 2020.
[31] A. G. Yepes, J. Doval-Gandoy, and H. A. Toliyat, "Multifrequency current control including distortion-free saturation and antiwindup with enhanced dynamics," *IEEE Trans. Power Electron.*, vol. 33, no. 9, pp. 7309–7313, Sep. 2018.
[32] A. G. Yepes and J. Doval-Gandoy, "Simple carrier-based PWM for prolonged high dc-link utilization for symmetrical and asymmetrical n-phase ac drives," *IEEE Trans. Power Electron.*, accepted for publication.
[33] A. S. Abdel-Khalik, R. A. Hamdy, A. M. Massoud, and S. Ahmed, "Postfault control of scalar (V/f) controlled asymmetrical six-phase induction machines," *IEEE Access*, vol. 6, pp. 59 211–59 220, 2018.
[34] C. Zhou, G. Yang, and J. Su, "PWM strategy with minimum harmonic distortion for dual three-phase permanent-magnet synchronous motor drives operating in the overmodulation region," *IEEE Trans. Power Electron.*, vol. 31, no. 2, pp. 1367–1380, Feb. 2016.
[35] S. Paul and K. Basu, "Overmodulation techniques of asymmetrical six-phase machine with optimum harmonic voltage injection," *IEEE Trans. Ind. Electron.*, vol. 68, no. 6, pp. 4679–4690, 2021.
[36] S. Paul and K. Basu, "A three-phase inverter based overmodulation strategy of asymmetrical six-phase induction machine," *IEEE Trans. Power Electron.*, vol. 36, no. 5, pp. 5802–5817, 2021.
[37] T. Komrska, T. Glasberger, and Z. Peroutka, "Overmodulation of seven-phase systems using minimum infinity norm," in *Proc. IEEE PEDS*, Dec. 2017, pp. 940–944.
[38] J. M., V. S. N., D. D., and L. E., "A synchronous current control scheme for multiphase induction motor drives," *IEEE Trans. Energy Convers.*, vol. 24, no. 4, pp. 860–868, Dec. 2009.
[39] C. H. S., L. E., J. M., H. W.-P., and R. N. A., "Current control methods for an asymmetrical six-phase induction motor drive," *IEEE Trans. Power Electron.*, vol. 29, no. 1, pp. 407–417, Jan. 2014.
[40] Y. A. G., M. J., V. A., L. O., and D.-G. J., "Current harmonics compensation based on multiresonant control in synchronous frames for symmetrical n-phase machines," *IEEE Trans. Ind. Electron.*, vol. 62, no. 5, pp. 2708–2720, May 2015.
[41] Y. Zhu, W. Gu, K. Lu, and Z. Wu, "Vector control of asymmetric dual three-phase PMSM in full modulation range," *IEEE Access*, vol. 8, pp. 104 479–104 493, 2020.
[42] D. Yazdani, S. Ali Khajehoddin, A. Bakhshai, and G. Joos, "Full utilization of the inverter in split-phase drives by means of a dual three-phase space vector classification algorithm," *IEEE Trans. Ind. Electron.*, vol. 56, no. 1, pp. 120–129, Jan. 2009.
[43] L. Harnefors and H. P. Nee, "Model-based current control of ac machines using the internal model control method," *IEEE Trans. Ind. Appl.*, vol. 34, no. 1, pp. 133–141, Jan./Feb. 1998.
[44] L. Harnefors, K. Pietilainen, and L. Gertmar, "Torque-maximizing field-weakening control: design, analysis, and parameter selection," *IEEE Trans. Ind. Electron.*, vol. 48, no. 1, pp. 161–168, Feb. 2001.
[45] Y. C. Kwon, S. Kim, and S. K. Sul, "Voltage feedback current control scheme for improved transient performance of permanent magnet synchronous machine drives," *IEEE Trans. Ind. Electron.*, vol. 59, no. 9, pp. 3373–3382, Sep. 2012.

Alejandro G. Yepes (S'10-M'12-SM'19) received the M.Sc. and Ph.D. degrees in electrical engineering from Universidade de Vigo, Vigo, Spain, in 2009 and 2011, respectively.

Since 2008, he has been working with the Applied Power Electronics Technology Research Group, Universidade de Vigo. From August 2016 to June 2018, he stayed with the Department of Electrical and Computer Engineering, Texas A&M University, College Station, TX, USA, after which he returned to Universidade de Vigo. His research interests are in the areas of ac power conversion, with special focus, currently, on multiphase drives.

Jesus Doval-Gandoy (M'99) received the M.Sc. and Ph.D. degrees in electrical engineering from the Polytechnic University of Madrid, Madrid, Spain, and from Universidade de Vigo, Vigo, Spain, in 1991 and 1999, respectively. He is a Professor and the Head of the Applied Power Electronics Technology Research Group (APET), Universidade de Vigo.

His research interests are in the areas of ac power conversion.